Alteration of cartilage mechanical properties in absence of β1 integrins revealed by rheometry and FRAP analyses

Carole Bougault, Livia Cueru, Jonathan Bariller, Marilyne Malbouyres, Anne Paumier, Attila Aszodi, Yves Berthier, Frédéric Mallein-Gerin, Ana-Maria Trunfio-Sfarghiu

Alteration of cartilage mechanical properties in absence of β1 integrins revealed by rheometry and FRAP analyses

Carole Bougault [a], Livia Cueru [b], Jonathan Bariller [b], Marilyne Malbouyres [a], Anne Paumier [a], Attila Aszodi [c], Yves Berthier [b], Frédéric Mallein-Gerin [a,1], Ana-Maria Trunfio-Sfarghiu [b,*,1]

[a] *Institut de Biologie et Chimie des Protéines, FRE3310 CNRS, Université de Lyon, 7 Passage du Vercors, F-69367 Lyon Cedex 07, France*
[b] *Université de Lyon, CNRS INSA-Lyon, LaMCoS UMR5259, F-69621, France*
[c] *Experimental Surgery and Regenerative Medicine, Department of Surgery, Ludwig-Maximilians-University (LMU), Nussbaumstr. 20, 80336 Munich, Germany*

Context: Mechanical properties are essential for biological functions of the hyaline cartilage such as energy dissipation and diffusion of solutes. Mechanical properties are primarily dependent on the hierarchical organization of the two major extracellular matrix (ECM) macromolecular components of the cartilage: the fibrillar collagen network and the glycosaminoglycan (GAG)-substituted proteoglycan, mainly aggrecan, aggregates. Interaction of chondrocytes, the only cell type in the tissue, with the ECM through adhesion receptors is involved in establishing mechanical stability via bidirectional transduction of both mechanical forces and chemical signals. In this study, we aimed to determine the role of the transmembrane β1 integrin adhesion receptors in cartilage biomechanical properties by the use of genetic modification in mice.

Methods: Costal cartilages of wild type and mutant mice lacking β1 integrins in chondrocytes were investigated. Cartilage compressive properties and solute diffusion were characterized by rheometric analysis and Fluorescence Recovery After Photobleaching (FRAP), respectively. Cartilage tissue sections were analyzed by histology, immunohistochemistry and transmission electron microscopy (TEM).

Results: At the histological level, the mutant costal cartilage was characterized by chondrocyte rounding and loss of tissue polarity. Immunohistochemistry and safranin orange staining demonstrated apparently normal aggrecan and GAG levels, respectively. Antibody staining for collagen II and TEM showed comparable expression and organization of the collagen fibrils between mutant and control cartilages. Despite the lack of gross histological and ultrastructural abnormalities, rheological measurements revealed that the peak elastic modulus in compression of mutant cartilage was 1.6-fold higher than the peak elastic modulus of wild-type sample. Interestingly, the diffusion coefficient within the mutant cartilage tissue was found to be 1.2-fold lower in the extracellular space and 14-fold lower in the pericellular (PCM) space compared to control.

Conclusion: The results demonstrate that the absence of β1 integrins on the surface of chondrocytes increases the stiffness and modifies the diffusion properties of costal cartilage. Our data imply that β1 integrins-mediated chondrocyte–matrix interactions directly affect cartilage biomechanics probably by modifying physical properties of individual cells. This study thus highlights the crucial role of β1 integrins in the cartilage function.

1. Introduction

Biomechanical properties of the load-bearing cartilaginous tissues have pivotal importance for the muscoskeletal system enabling organ protection and body movements. The hyaline cartilage is an avascular and aneural poroelastic material composed of fluid and solid (matrix) components. The extracellular matrix (ECM) of cartilage contains a number of macromolecular components including collagen fibers, proteoglycan aggregates and non-collagenous glycoproteins. The polyanionic, sulfated glycosaminoglycan (GAG) side chains of proteoglycans (mainly aggrecan) attract a large amount of water generating high osmotic (swelling) pressure within the tissue that resists compressive forces in weight-bearing cartilages. The aggrecan–water gel aggregates are embedded into a heteropolymeric collagen fibrillar network composed of major (type II) and minor (types IX and

* Correspondence to: Université de Lyon, CNRS INSA-Lyon, LaMCoS UMR5259, 18-20 rue des Sciences, F-69621 Villeurbanne Cedex, France.
Tel.: +33 4 72 43 72 45; fax: +33 4 78 89 09 80.
E-mail address: ana-maria.sfarghiu@insa-lyon.fr (A.-M. Trunfio-Sfarghiu).
[1] FMG and AMTS: equal contribution.

XI) collagens. The intrinsic stiffness of the collagen molecules and the extensive cross-linking between the fibrils provide the meshwork with tensile strength and restraining stress that counteracts tissue swelling. The delicate balance between swelling pressure and restraining stress controls the mechanical properties of cartilage (Cohen et al., 1998), which in turn are essential for articulation, loading, energy dissipation and diffusion of solutes. Dissipation of mechanical energy in articular cartilage subjected to dynamic loads during gait is essential to protect bone structures from mechanical stress in joints. Likewise, diffusion is fundamental for transporting nutrients, oxygen, waste products, and signaling molecules in cartilage owing to the avascular nature of the tissue.

Chondrocytes, the sole cell type that resides in the cartilage, are responsible for the synthesis, maintenance and degradation of the ECM components. Chondrocytes, with increasing distance from the cell surface, are surrounded by pericellular, territorial and interterritorial matrix compartments characterized by distinct composition and organization of the ECM macromolecules (Buckwalter and Mankin, 1998). On chondrocytes, various receptors interact with either soluble (growth factors) or solid (matrix) molecules in the pericellular zone. Adhesion molecules like integrins, annexin V, CD44 and discoidin domain receptors bind a range of ECM components, which trigger intracellular signaling cascades influencing the chondrocyte behavior such as proliferation, survival, polarity, gene expression, matrix synthesis and deposition. Integrins are a key class of cell adhesion molecules that connect the ECM to the cytoskeleton and mediate chemical as well as mechanical signals in and out of the cells. They are composed of α and β subunits and chondrocytes express specifically high levels of β1 integrin-containing heterodimers on their surface (Loeser, 2000). To assess the functions of β1 integrins in cartilage, transgenic mice, where β1 integrin gene (*Itgb*1) has been conditionally ablated in chondrocytes, were generated (Aszodi et al., 2003). Most of these mice develop perinatal lethal chondrodysplasia characterized by chondrocyte proliferation, shape and polarity defects, as well as moderate ultrastructural abnormalities of the collagen fibrillar network in the developing cartilaginous skeleton. Similar phenotype was found in the adult articular cartilage upon limb mesenchyme-specific deletion of *Itgb*1 (Aszodi et al., 2003).

In the present study, we aimed to determine if β1 integrins play a role in cartilage biomechanical properties comparing *Itgb*1$^{fl/fl}$–*Col2a1cre* (mutant) cartilage with normal cartilage obtained from wild-type (WT) mice. Since *Itgb*1 deletion in chondrocytes causes early lethality, we isolated cartilage explants from embryonic rib cage, the most abundant source of cartilage in the mouse embryo. Cartilage compressive properties were characterized by the peak elastic modulus in compression at the tissue-scale by rheometric analysis. Fluorescence Recovery After Photobleaching (FRAP) was performed to determine diffusion properties upon fluorescent dextran loading. The biochemical composition of cartilage matrix was analyzed by immunohistochemistry and its ultrastructural organization by transmission electron microscopy (TEM). We found that the lack of β1 integrin impairs the stiffness and diffusion properties of costal cartilage implying an important role of β1 integrin heterodimers in cartilage biomechanics.

2. Materials and methods

2.1. Conditional knockout mice and preparation of cartilage samples

To obtain mice lacking β1 integrins in cartilage, we crossed mice carrying the floxed *β1 integrin* (*Itgb*1^{fl}) gene (Potocnik et al., 2000) with mice expressing the cre recombinase under the control of regulatory regions the mouse collagen type II (*Col2a*1) gene (Sakai et al., 2001). Costal cartilage was isolated from the ventral parts of the rib cage of wild type (WT) and mutant (*Itgb*1$^{fl/fl}$–*Col2a*1*cre*) mice at 17.5-days post-coitum (17.5-dpc) (Fig. 1). For rheometry, FRAP and TEM analyses, cartilage explants were isolated from the two lowest non-floating ribs. These two ribs offer the advantage of being the longest and having similar geometry. Ablation of the *Itgb*1 allele was associated with activation of a promoterless *lacZ* reporter gene (Potocnik et al., 2000) allowing to monitor deletion efficiency with X-gal staining as described by Lefebvre et al. (1994). The costal cartilage samples were analyzed within 4 days following their isolation. They were stored at 4 °C in phosphate buffered saline solution (PBS) at pH 7.4, with antibiotics (penicillin (1000 U/mL) and streptomycin (0.1 mg/mL), Gibco) until mechanical testing.

2.2. Real-time PCR analysis

The absence of *β1 integrin* mRNA expression was confirmed by using a real-time PCR. Chondrocytes were isolated from costal cartilage as described by Bougault et al. (2009). Total RNA was extracted from isolated cells by the Nucleospin RNA II kit according to the manufacturer instructions (Macherey-Nagel). For cDNA synthesis, 1 μg of total mRNA and SuperScriptTM II Reverse Transcriptase (Invitrogen) were used. Real-time PCR reactions were performed in an I-Cycler apparatus (Biorad) using an iQ SYBR Green Supermix (Biorad) and primer pairs specific for *β1 integrin* (*Itgb*1), *α10 integrin* (*Itga*10) and the internal standard *ribosomal protein L13a* (*Rpl*13*a*). The primer sequences were:

*Itgb*1 s-ATGCAGGTTGCGGTTTGT, as-CATCCGTGGAAAACACCAG
*Itga*10 s-ATGGCTGCTCTTCCTGATCT, as-CTGAACTGCTGACCTGGGTA
*Rpl*13*a* s-ATCCCTCCACCCTATGACAA, as-GCCCCAGGTAAGCAAACTT.

2.3. Mechanical tests using a rheometric system

The mechanical resistance of the cartilage samples was measured by compression testing in an unconfined configuration. Step-wise compression tests were performed with an Advanced Rheometric Expansion System (ARES, TA Instruments). In order to control the boundary conditions, the platens were sonicated twice for 10 min at 25 °C in ethanol, before use. The costal cartilage was placed in the center of a 10 μL drop of PBS to maintain sample hydration. In order to have a uniform contact area and thickness for all samples, a pre-load of 0.01 N was applied under a rheometer. The samples were then allowed to relax for 5 min. After this relaxation, the normal stress level measured by the rheometer was close to 0, so that initial conditions were similar for all samples. A total of 18 cartilage samples were used for the step-wise compression tests ($n=8$ for WT and $n=10$ for mutants).

The thickness of each pre-loaded sample was noted before rheological tests. For the contact area measurement, the pre-load of 0.01 N was applied with a thin glass

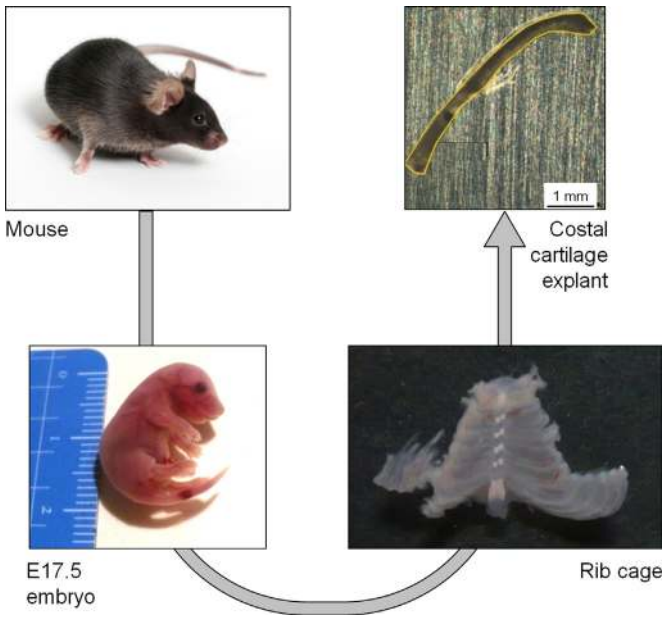

Fig. 1. Preparation of the cartilage explants. Experimental procedure diagram of the cartilage preparation. Cartilage was isolated from the ventral part of rib cages of mouse embryos at 17.5-dpc. Top right: optical image of a cartilage sample under a thin glass plate weighing 1 g (viewed from the top). This image was used to monitor the contact area and the initial thickness of pre-load samples (0.01 N) before the rheological stress–relaxation tests (scale bar 1 mm).

plate (1 g) under a binocular microscope (Fig. 1). In addition, we tested the uniformity of the thickness under a confocal microscope, by measuring the width of the pre-loaded samples at 10 different points.

2.4. Mechanical data acquisition and analysis

Starting from the initial condition (0.01 N pre-load), a cycle of five strains were performed with an imposed speed deformation of 0.02 mm/s and a compression level representing 10% of the sample thickness. Every compression strain ramp was followed by a period of stress relaxation of 250 s to reach the balance of stress equilibrium characteristic of biphasic materials. The normal force and the gap thickness were directly measured by the rheometer sensors. Stress–relaxation curves were generated for each sample: compressive and relaxation stresses, calculated as normal force divided by the costal cartilage area, were drawn as functions of time (Fig. 2).

Stress–strain curves were generated by taking only into consideration the compression peak stress, where the compressive strain (ε) was calculated as

$$\varepsilon = \frac{h_0 - h_i}{h_0} \tag{1}$$

where h_0 is the initial gap (pre-load) and h_i is the controlled gap.

According to Hooke's law, the linear regression slope for the significant compressive peaks of stress–strain curve was used to estimate the peak compression modulus (E^*) for each cartilage sample.

2.5. Diffusion tests using Fluorescence Recovery After Photobleaching (FRAP)

Fluorescence Recovery After Photobleaching (FRAP) was applied for measuring the molecular diffusion speed with a confocal microscope (Axelrod et al., 1976). We used 70 kDa dextran labeled with neutral fluorescein (Sigma) at 0.1 mg/mL in PBS. Each cartilage sample was immersed in the fluorescein-labeled 70 kDa dextran solution at 4 °C for at least 48 h prior to FRAP measurements, to allow the system to equilibrate and to allow dextran to fully permeate the cartilage matrix.

Samples were sandwiched between glass coverslips and were kept moist in the labeling solution during the FRAP experiments. FRAP measurements were performed on a TCS SP5 Leica confocal microscope using a 63 × 1.20 water objective. Photobleaching was performed with an argon laser at 70% laser power and at 100% transmission and imaging with the same laser at 15% transmission (to prevent bleaching). Circular areas were uniformly bleached (regions of interest are termed ROI). Each sample was analyzed in multiple zones (2–20 ROI). ROI's size of 50 or 100 μm diameter was used to estimate diffusion in the matrix or solution. 10 μm diameter ROI was used to estimate diffusion at the PCM level (Fig. 3A). Eight cartilage explants were tested ($n=3$ for WT and $n=5$ for mutants). For each experiment, approximately 250 images were acquired at 1.32 s intervals, including three pre-bleach images, 50 bleach images and between 150 and 200 post-bleach images (the post-bleach time was adjusted to achieve the highest degree of fluorescence recovery), to track the fluorescence recovery. The pre-bleach images

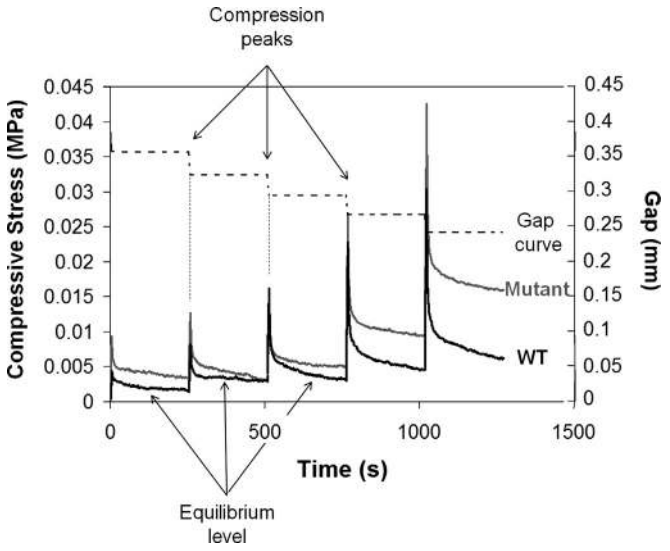

Fig. 2. Stress–relaxation test. Stress–relaxation responses of WT and mutant cartilage explants under unconfined compression. A cycle of five strains were applied; each compression (reaching 10% of the sample thickness) was followed by a period of stress–relaxation of 250 s (dotted line). Stress–relaxation curves were generated; compressive stress (normal force divided by the costal cartilage area) was plotted as a function of time for WT (black line) or mutant (gray line) samples.

are used to establish the initial intensity for normalization of the data series (Fig. 3B). For each experiment, a fluorescent dextran solution of 0.1 mg/mL in PBS was also subjected to FRAP analysis, as control. All measurements were made at room temperature (25 ± 1 °C).

2.6. Diffusion data acquisition and analysis

Fluorescent intensity analysis of FRAP experiments was performed on the basis of the manufacturer's handbook of the confocal microscope (Leica, Eq. (2)). For each photobleached zone, a "reference ROI" not subjected to photobleaching was recorded. The fluorescence intensity of the experimental curve ($I_{ROI}(t)$) was divided by a correction factor in order to bring the I_{ROI} at the same pre-bleached intensity level as the reference ROI ($I_{reference}$) at initial conditions. Thus, the correction factor corresponds to the ratio of the initial fluorescence intensity (pre-bleached intensity, $I_{(0)}$) of the experimental curve to the reference curve. The corrected I_{ROI} was subtracted from the reference curve's fluorescent intensity ($I_{reference}(t)$) in order to eliminate the photobleaching due to image acquisition. The result is represented as a curve $f_d(t)$ that we call "normalized difference fluorescence intensity" (Fig. 3C).

$$f_d(t) = I_{reference}(t) - \frac{I_{ROI}(t)}{I_{ROI}(0)/I_{reference}(0)} \tag{2}$$

The normalized difference fluorescence intensity curve was fitted using an exponential mathematical law (Fig. 3C):

$$y(t) = ae^{-t/b} + c \tag{3}$$

The equation for the curve was used to determine the half-recovery time ($t_{1/2}$):

$$t_{1/2} = \ln 2b \tag{4}$$

The half-recovery time ($t_{1/2}$), and the radius of the photobleached area (w) were used to determine the diffusion coefficient (D), using the following simplified equation (Axelrod et al., 1976):

$$D = \frac{w^2}{4t_{1/2}} \tag{5}$$

2.7. Cell viability

Cell death within the costal cartilage was measured using the Cytotoxicity Detection Kit (Roche Applied Science), as described by the manufacturer. Absorbance was measured at 490 nm. Samples representing 100% viability were stored only for 1 day. Samples representing 100% mortality were treated with Triton X100 (Sigma Aldrich) 1% in PBS.

2.8. Histological analysis of the cartilage matrix

For histological analysis, costal cartilage explants were fixed in 4% formaldehyde (pH 7.4) for 24 h at 4 °C. The samples were embedded in paraffin, sectioned at 7 μm and stained with Mayer's hematoxylin. For histochemical detection of sulfated proteoglycans, sections were stained with 0.5% safranin-O in 0.1 M sodium acetate at pH 7.4 for 10 min. Safranin-O is a cationic dye that binds GAGs and stains orange in an aqueous mounting medium (Rosenberg, 1971). Mayer's hematoxylin staining was used to counterstain nuclei in chondrocytes. Immunofluorescence detection of type II collagen and aggrecan in the ECM was performed as previously described by Bougault et al. (2009).

2.9. Ultrastructural analysis of the cartilage matrix

Costal cartilage explants were fixed at room temperature in a mixture of 2.5% glutaraldehyde and 2% paraformaldehyde (EM grade, Delta Microscopies) in 0.2 M sodium cacodylate buffer (pH 7.4) for 2 h. After rinsing in 0.15 M sodium cacodylate, explants were post-fixed with 1% osmium tetroxide in 0.1 M sodium cacodylate for 45 min. Samples were then dehydrated in graded series of ethanol (from 30 to 100%), and embedded in epoxy resin as previously described by Chanut-Delalande et al. (2004). Ultra-thin, 70 nm sections were cut using a Leica UC7 ultramicrotome. The sections were treated with 7% uranyl acetate in methanol and lead citrate, and then examined with a Philips CM120 electron microscope equipped with a Gatan Orius 200 2K × 2K digital camera ("Centre Technologique des Microstructures", Université Lyon I, Villeurbanne, France).

2.10. Statistical analysis

The data are expressed as the mean ± standard deviation (SD). Statistical significance was assessed using the Student T-test and $p < 0.05$ was considered significant.

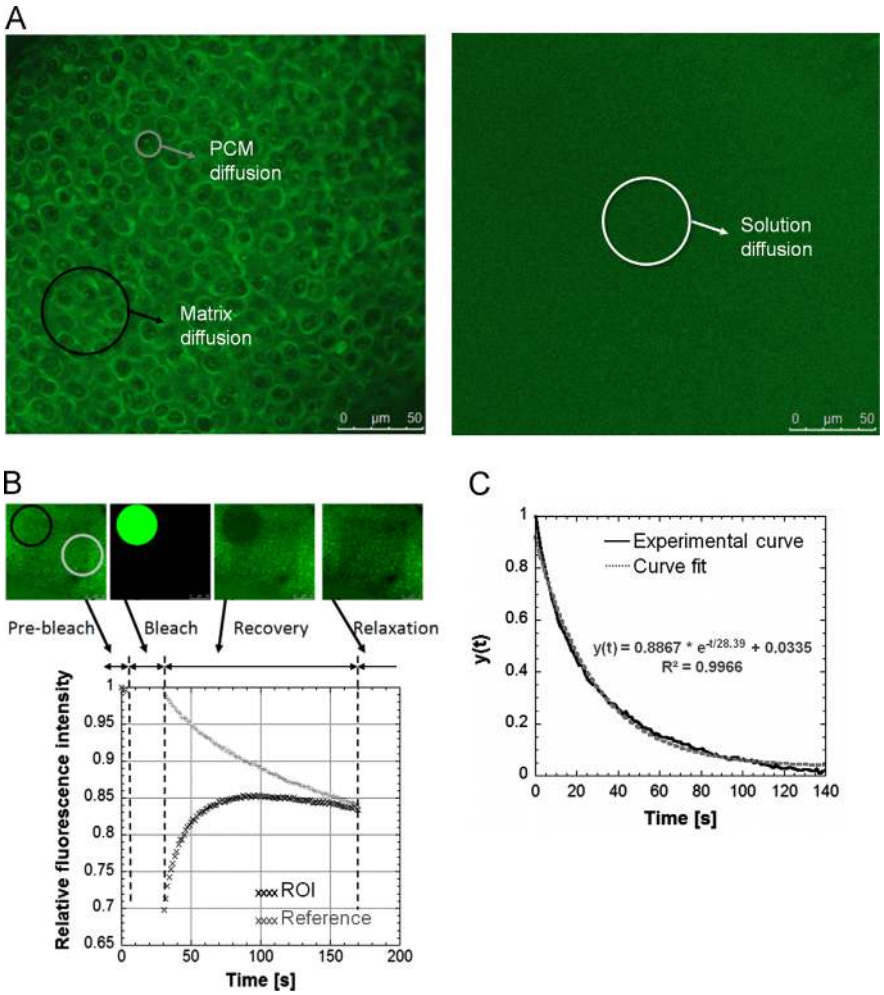

Fig. 3. FRAP diffusion tests. (A) Confocal fluorescence image of a cartilage sample (on the left) or reference solution (on the right) before FRAP analysis. ROI with 10 μm diameter (gray circle) was used to measure PCM diffusion, while ROI with 50 μm diameter (black circle) was used to measure matrix diffusion. (B) Diagram of the FRAP experimental procedure (top) and curve of fluorescence recovery after photobleaching of costal cartilage with 100 μm diameter ROI (bottom). Relative fluorescence intensity was plotted as a function of time for bleached ROI (black line) and non-bleached reference (gray line). (C) Adjusted regression curve (100 μm diameter ROI) for costal cartilage (black line), fitted with the displaced exponential law (gray dotted line). The exponential equation of the fitted curve and the coefficient of determination is indicated.

3. Results

3.1. Absence of β1 integrins in mutant cartilage and ECM analysis

Costal cartilages of 17.5-dpc WT and mutant mice were first investigated for the expression of β1 integrin. X-gal staining showed LacZ activity in all mutant chondrocytes implicating a highly efficient deletion of the floxed *Itgb*1 gene (Fig. 4A). RT-PCR analysis of total RNA isolated from chondrocytes revealed the complete lack of *Itgb*1 mRNA in mutant samples. The expression of the *Itga*10 mRNA encoding the α10 subunit of the collagen-binding α10β1 integrin heterodimer was comparable between the genotypes (Fig. 4B). Next, the structure and composition of cartilage samples were analyzed by histology, immunohistochemistry and electron microscopy. Hematoxylin staining highlighted a marked change in cell shape of β1 integrin-deficient costal cartilage. Mutant chondrocytes appeared clearly more rounded and larger than normal chondrocytes (Fig. 5A). Safranin-O staining for the negatively charged GAG chains and immunofluorescence staining using antibodies against the aggrecan and type II collagen demonstrated normal proteoglycan and collagen deposition in mutant compared to WT (Fig. 5B–D). Moreover, TEM analysis revealed similar ultrastructural organization of the collagen/proteoglycan network in WT and mutant (Fig. 5E). Collectively, the data suggest that synthesis and deposition of the major ECM macromolecules are apparently unaffected by the lack of β1 integrins in 17.5-dpc costal cartilage.

3.2. The lack of β1 integrins alters the compressive properties of cartilage

To assess the role of β1 integrins in the mechanical properties of cartilage, stress–relaxation tests were performed on WT and β1 mutant costal cartilage samples. First, we verified that cell viability within the explants was not altered by our storage conditions. The maximum cytotoxicity was estimated at $6 \pm 1\%$ ($n=5$), which was considered negligible. Next, we characterized the geometry of the samples before compression tests, with a pre-load of 0.01 N. The average contact area was 1.90 ± 0.48 mm² for WT, and 1.79 ± 0.45 mm² for mutant samples ($n=10$). The average thickness of the pre-loaded samples (the initial gap noted h_0 in Eq. (1)) was 211 ± 44 μm for WT, and 195 ± 41 μm for mutant ($n=10$). The reduced size of the mutant samples was expected because of the abnormalities in the developing cartilaginous skeleton already described in the mutant mice (Aszodi et al., 2003). In addition, within the same pre-loaded sample, the variation in width was between 6% and 10% ($n=9$). Importantly, the difference of thickness between samples did not affect the peak compression

modulus (E^*) because it was calculated taking into account the ratio dh/h_0. Similarly, the difference of contact area between samples was heeded because the compressive stresses were calculated as normal force divided by the sample area.

Concerning the step-wise compression tests, the means of peak intensities, representing the immediate response to compression, were significantly different for the WT and mutant explants (Fig. 6A). The corresponding peak elastic moduli (E^*) were 32.7 ± 0.01 kPa for the WT samples ($n=8$) and 53.7 ± 0.02 kPa for the mutant samples ($n=10$); thus the relative E^* of the mutant cartilage was approximately 1.6-fold higher compared to WT ($p=0.018$, Fig. 6B). The result indicates that the compressive

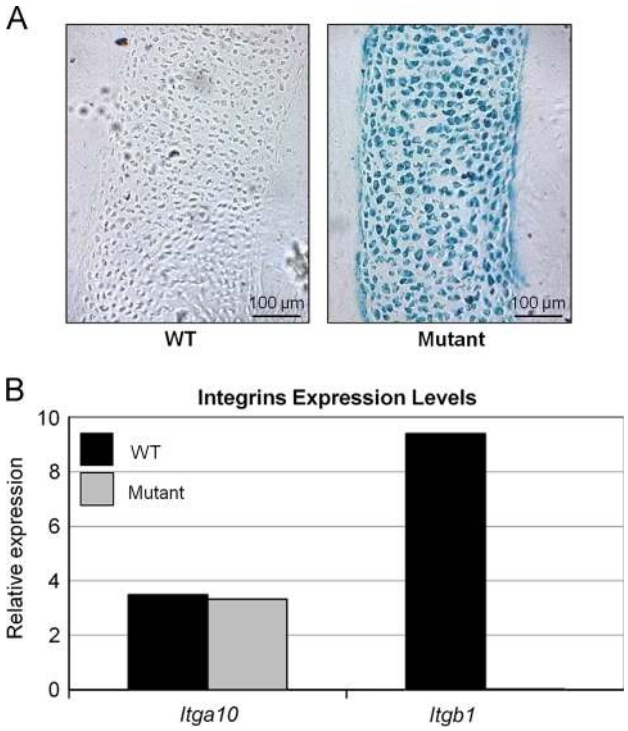

Fig. 4. Validation of the absence of β1 integrins in the mutant costal cartilage. (A) X-gal staining of costal cartilage sections from wild type (WT) and mutant embryos. Blue cells show LacZ activity demonstrating the deletion of the *β1 integrin* gene. (B) The real-time PCR confirms the loss of *β1 integrin* (*Itgb*1) expression in mutant chondrocytes (right), while *α10 integrin* (*Itga*10) is expressed by both mutant and WT cells. (For interpretation of the references to color in this figure legend, the reader is referred to the web version of this article).

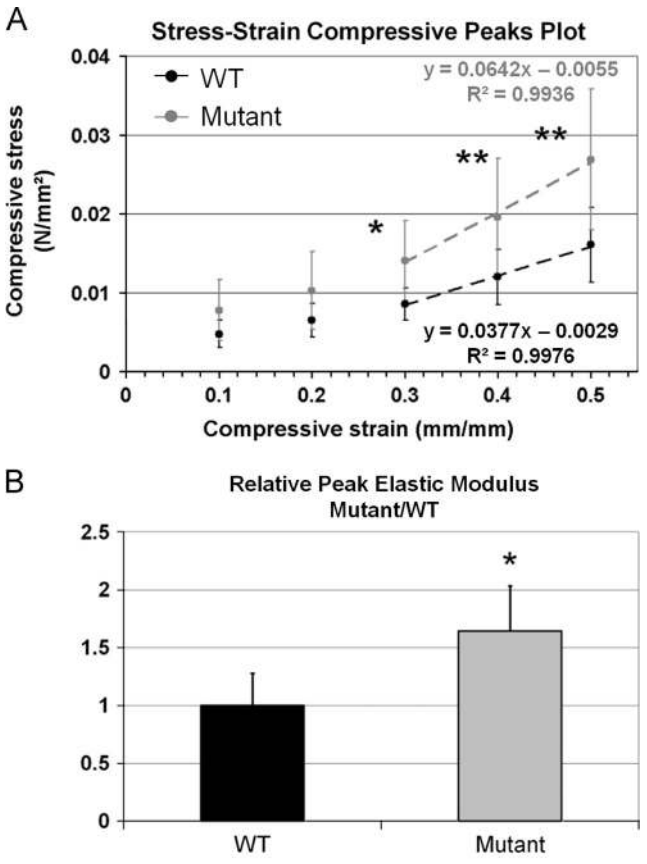

Fig. 6. Higher peak elastic modulus in mutant cartilage compared to wild type (WT) cartilage. (A) Stress–strain compressive peaks plot for WT (black line) and mutant (gray line) cartilage samples. Corresponding linear regression slopes for the significant compressive peaks of stress–strain curve are plotted as dotted lines; and linear equations and coefficients of determination are indicated on the right. Slope coefficient was used to estimate the apparent elastic modulus of each costal cartilage (mean ± SD, $^*p < 0.05$, $^{**}p < 0.01$, mutant versus WT).(B) Relative peak elastic modulus for mutant (gray bar) and WT (black bar) cartilage samples (mean ± SD, $^*p < 0.05$, mutant versus WT).

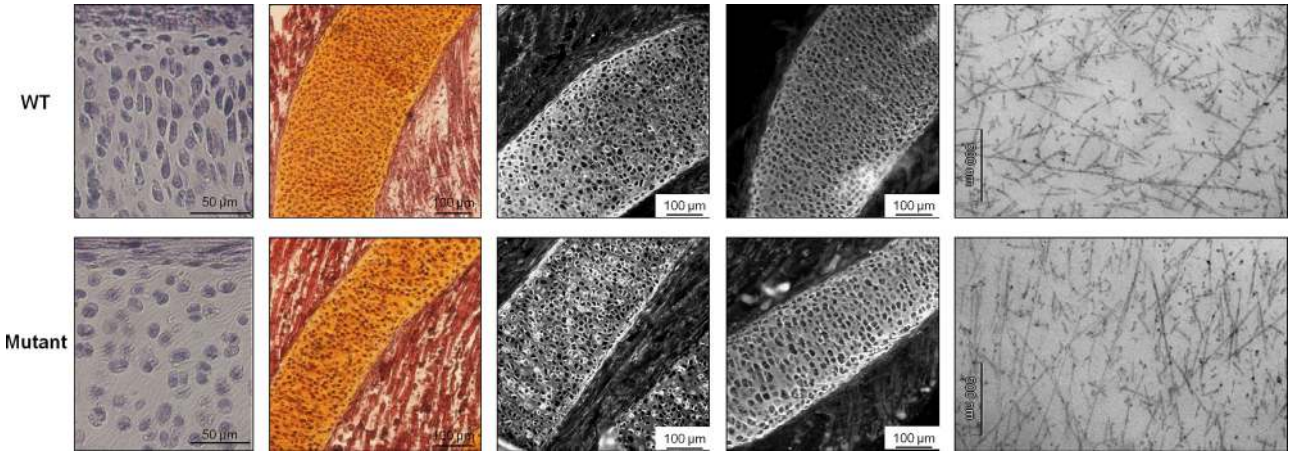

Fig. 5. The lack of β1 integrins in costal cartilage has no apparent affect on the deposition and organization of proteoglycans and collagens in the ECM. (A) Hematoxylin staining of longitudinal sections of rib cartilage demonstrates the flattened shape of wild type (WT) chondrocytes; whereas mutant chondrocytes appear more rounded. (B) Safranin-O staining shows comparable levels of sulfated proteoglycans in the ECM of WT and mutant cartilages. (C) Immunofluorescence detection of aggrecan. (D) Immunofluorescence detection of type II collagen. (E) TEM imaging reveals no obvious ultrastructural abnormalities in mutant cartilage compared to WT. The collagen network appears as thin fibers, dark dots represent proteoglycans aggregated on the collagen fibers after chemical fixation (scale bar 500 nm).

properties of cartilage are altered in absence of β1 integrins. This difference could be explained by the biphasic structure of cartilage, composed of a poroelastic solid phase represented by the matrix and the cells, and a uncompressible fluid phase represented by interstitial water and dissolved electrolytes (Ateshian, 1997). In order to investigate whether the mechanical difference was due to the solid or the fluid phase, we next examined diffusion properties of the WT and mutant cartilages.

3.3. Alteration of cartilage diffusion in absence of β1 integrins

FRAP experiments were performed on costal cartilage explants isolated from WT and mutant mouse embryos. The cytotoxicity after 4 days of storage was negligible and was not further increased by incubation with the fluorescein-labeled 70 kDa dextran solution ($4 \pm 1\%$, $n=5$). In WT cartilage, the matrix diffusion coefficient was estimated to be $7.7 \pm 0.6\ \mu m^2/s$ and the PCM diffusion coefficient was estimated to be $2.6 \pm 0.8\ \mu m^2/s$. Both coefficients were significantly lower in mutant cartilage (Fig. 7). Noticeably, the decrease of the mutant values was much more pronounced at the PCM level (14-fold decrease, $p=10^{-13}$) than at the ECM level (1.2-fold decrease, $p=0.007$). Thus, the diffusion properties of cartilage seem altered in absence of β1 integrins, particularly at the level of the surrounding PCM.

4. Discussion

The aim of the present study was to evaluate the impact of β1 integrin-deficiency on the mechanical behavior of rib cartilage isolated from genetically modified mouse embryos. Our results show that the peak elastic modulus (E^*) of embryonic costal cartilage assessed by unconfined compression is about 30 folds lower than the values found in literature for the mature human articular cartilage (Boschetti and Peretti, 2008). This discrepancy can be explained either by species- and location-specific differences of the cartilage or by the fact that the immature cartilage has about twice the cellularity of mature cartilage (Jadin et al., 2005). Importantly, we observed 1.6-fold increase of E^* in the mutant samples implicating that the adhesion receptor β1 integrins influence cartilage mechanical properties at cellular and/or extracellular matrix levels.

Cellularity of mouse cartilages is high compared to larger species such as bovine and man (Stockwell, 1972), therefore chondrocytes might significantly contribute to the bulk mechanical properties of the tissue. Histological analysis of costal cartilage has confirmed a shape change of chondrocytes from flattened and oriented (wild type) to rounded and non-oriented (mutant) phenotype in agreement with previous studies published on β1 integrin-deficient cartilages (Aszodi et al., 2003; Raducanu et al., 2009). The cytoplasmic tail of β1 integrins binds to the cytoskeleton via adapter proteins (Kaapa et al., 1999; Otey et al., 1993) forming an essential link between the ECM and inside of the cell. The bidirectional, matrix–integrin–cytoskeleton connection is fundamental for the chondrocyte geometry through the control of matrix attachment and organization of the cortical actin ring beneath the plasma membrane (Aszodi et al., 2003). Uncoupling the cytoskeleton and cell membrane in β1 integrin-deficient chondrocytes may result in a decrease of cellular deformability and an increase of cellular rigidity due to alterations of the cytoskeletal mechanics (Fig. 8). To validate this hypothesis, cell-scaled experiments should be considered to study more precisely the mechanical properties of individual chondrocytes isolated from WT and mutant cartilages.

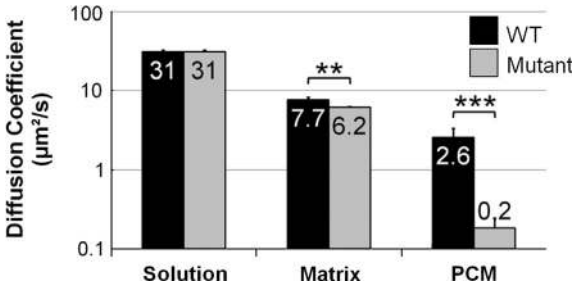

Fig. 7. Lower diffusion coefficient in mutant cartilage compared to wild type (WT) cartilage. Diffusion coefficient calculated from FRAP tests on mutant (gray bars) and WT (black bars) cartilage samples using fluorescein-labeled 70 kDa dextran 0.1 mg/mL in PBS. Matrix and solution diffusion coefficients were calculated for ROI to be 50 and 100 μm diameters respectively, and PCM diffusion coefficients were calculated for ROI to be 10 μm diameter (mean ± SD, $^{**}p < 0.01$, $^{***}p < 0.001$, mutant versus WT).

The macroscale biomechanical properties of the cartilage matrix are attributed primarily to the collagen fibrillar meshwork and the negatively charged proteoglycan aggrecan. In accordance with a previous study on embryonic limb cartilage (Aszodi et al., 2003), we found no obvious alterations in type II collagen or aggrecan deposition and organization in β1 integrin mutant costal cartilage by immunohistochemistry and TEM. Important to note, however, that adult cartilages lacking β1 integrins on chondrocytes display ultrastructural abnormalities characterized by changes in the density and diameter of collagen fibrils (Aszodi et al., 2003; Raducanu et al., 2009). Thus, we cannot exclude the possibility that mild structural changes in the fibrillar network of 17.5-dpc costal cartilage, which could be masked by the harsh chemical fixation and embedding procedure of the specimens for TEM analysis, contribute to the increased stiffness of mutant samples. Alternatively, higher GAG content can lead to higher stiffness in cartilage (Guilak et al., 1999). In our study, histochemical staining for GAGs with safranin-O indicated no significant difference in the amount of sulfated proteoglycans between wild type and mutant cartilages, however, this staining modality does not precisely reflect the GAG/proteoglycan content of the cartilage ECM (Camplejohn and Allard, 1988). Similarly, the chemical fixation used for TEM precipitates proteoglycans, thus the original proteoglycan network cannot be estimated by the conventional ultrastructural analysis.

Diffusion of solutes in cartilage is dependent on specific properties of the solute and the ECM; thus the mobility of a particular solute can correlate with the composition, structure and biomechanics of the tissue. For example, proteoglycan depletion in articular cartilage by enzymatic digest increases diffusivity of large uncharged solutes such as 70 kDa dextran (Torzilli et al., 1997) and reduces compressive stiffness (Guterl et al., 2009). To explain the different mechanical behaviors between wild-type and mutant costal cartilage samples, the diffusion coefficient of fluorescein-labeled 70 kDa dextran within the ECM and PCM was measured using the FRAP technique (Fetter et al., 2006). The large bleach spots (50 or 100 μm diameter) were used to estimate the diffusion in the ECM, where the contribution of the cells can be neglected (Maroudas, 1970, 1979). The diffusion coefficient of $7.7 \pm 0.6\ \mu m^2/s$ that we measured in mouse cartilage matches well with the literature data. For example, using the FRAP technique, the diffusion coefficient of 70 kDa dextran in pig cartilage was estimated at $3.8\ \mu m^2/s$ (Greene et al., 2008) and using the pulsed field gradient NMR technique, the diffusion coefficient of 70 kDa dextran in bovine cartilage was measured as $3\ \mu m^2/s$ (Trampel et al., 2002). Our results revealed that the diffusion coefficient was only slightly lower in the matrix of mutant cartilage compared to WT. This observation hence argues against significant changes in the composition and/or structure of the mutant cartilage ECM.

Next, we used smaller bleach spots (10 μm diameter) to assess diffusivity at the pericellular matrix (PCM) level and found 3-fold

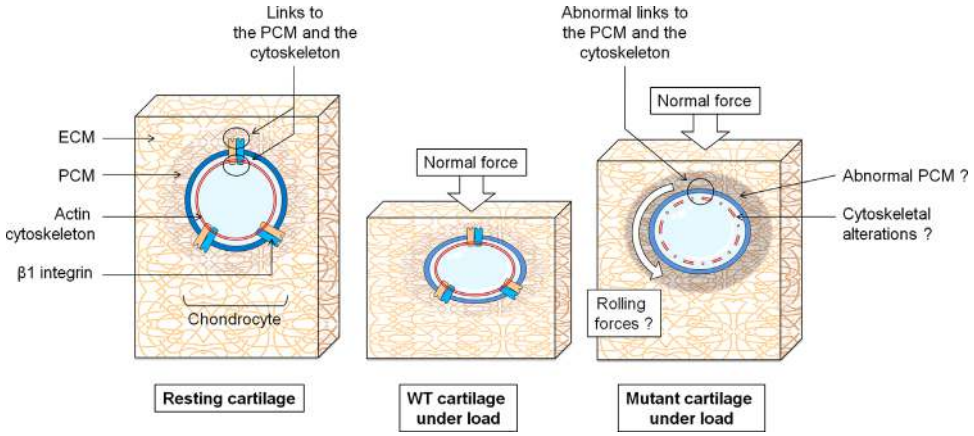

Fig. 8. Alterations of biomechanical properties of individual chondrocytes lacking β1 integrins may cause an increase in rigidity at the tissue level. The deformation of mutant cartilage explants in response to normal force is lower compared to wild-type samples. We suggest that the increased compressive stiffness of cartilage lacking β1 integrins is caused by decrease in matrix permeability and possibly by increase in rigidity of each chondrocyte. The alterations of cellular biomechanical properties may be due to defects in cytoskeleton–cell–matrix interactions. The normal forces applied to the cartilage explants could partially convert into rolling forces around chondrocytes lacking β1 integrin receptors.

lower diffusion coefficient compared to ECM in the wild-type specimen. In agreement, the PCM surrounding the chondrocytes was shown significantly less permeable than the distant inter-territorial matrix in healthy bovine cartilage using the FRAP method (Irrechukwu, 2007). However, FRAP may not be the more appropriate method to estimate the diffusion at the PCM level because of the inadequate initial and boundary conditions (Axelrod et al., 1976). Yet, similar results were obtained using the accurate technique of 3D scanning microphotolysis: the diffusivity of the PCM in healthy porcine articular cartilage was shown 1.2-fold lower than that of the adjacent ECM, with 70 kDa dextran (Leddy et al., 2008). The difference in diffusivity between PCM and ECM is likely attributable to the differences in the structure and composition of the PCM, which contains finer collagen fibers and a higher concentration of proteoglycans relative to the ECM (Poole et al., 1988).

The great difference of diffusion coefficient at PCM level between mutant and wild-type (14-fold reduction) suggests less permeability of the PCM to macromolecular florescent solutes (~8 nm radius of gyration) in mutant specimen. β1 integrins interact with various matrix proteins of the cartilage (Loeser, 2000; Wickstrom and Fassler, 2011), therefore β1 integrin-deficiency may affect the composition and/or organization of the PCM (Buckwalter and Mankin, 1998; Loeser, 1997; Poole et al., 1988). Indeed, we have previously reported that the PCM compartment is enlarged and has reduced collagen VI content in β1-null articular cartilage (Raducanu et al., 2009). Such alterations may decrease the friction coefficient between cell and PCM, which in turn changes the boundary conditions for the mechanical behavior. This change might correlate with chondrocyte morphology in the tissue. Wild-type chondrocytes are more flattened than mutants owing to the importance of integrin-mediated interactions on cell deformation induced by internal mechanical stress (Fig. 8).

5. Conclusion

Taken together, our results demonstrate that disturbing the cytoskeleton–cell–matrix interactions by deleting integrin β1 receptors in chondrocytes alters the biomechanical properties of cartilage. The observed increase in compressive stiffness at the tissue level is most likely caused by alterations in the mechanical behavior of the cells and/or the PCM. This study unravels the crucial role of β1 integrins in the mechanical properties of cartilage.

Author contributions

Study design: CB, LC, YB, FMG, and AMTS.
Acquisition of data: CB, LC, JB, MM, and AP.
Analysis and interpretation of data: CB, LC, AA, JB, AP, and AMTS.
Manuscript preparation: CB, LC, AA, YB, FMG, and AMTS.

Conflict of interest

The authors declare no conflict of interest.

References

Aszodi, A., Hunziker, E.B., Brakebusch, C., Fassler, R., 2003. Beta1 integrins regulate chondrocyte rotation, G1 progression, and cytokinesis. Genes and Development 17 (19), 2465–2479.
Ateshian, G.A., 1997. Finite deformation biphasic material properties of bovine articular cartilage from confined compression experiments. Journal of Biomechanics 30, 1157–1164.
Axelrod, D., Koppel, D.E., Schlessinger, J., Elson, E., Webb, W.W., 1976. Mobility measurement by analysis of fluorescence photobleaching recovery kinetics. Biophysical Journal 16 (9), 1055–1069.
Boschetti, F., Peretti, G.M., 2008. Tensile and compressive properties of healthy and osteoarthritic human articular cartilage. Biorheology 45 (3–4), 337–344.
Bougault, C., Paumier, A., Aubert-Foucher, E., Mallein-Gerin, F., 2009. Investigating conversion of mechanical force into biochemical signaling in three-dimensional chondrocyte cultures. Nature Protocols 4 (6), 928–938.
Buckwalter, J.A., Mankin, H.J., 1998. Articular cartilage: tissue design and chondrocyte–matrix interactions. Instructional course lectures 47, 477–486.
Camplejohn, K.L., Allard, S.A., 1988. Limitations of safranin 'O' staining in proteoglycan-depleted cartilage demonstrated with monoclonal antibodies. Histochemistry 89 (2), 185–188.
Chanut-Delalande, H., Bonod-Bidaud, C., Cogne, S., Malbouyres, M., Ramirez, F., Fichard, A., Ruggiero, F., 2004. Development of a functional skin matrix requires deposition of collagen V heterotrimers. Molecular and Cellular Biology 24 (13), 6049–6057.
Cohen, N.P., Foster, R.J., Mow, V.C., 1998. Composition and dynamics of articular cartilage: structure, function, and maintaining healthy state. Journal of Orthopaedic and Sports Physical Therapy 28 (4), 203–215.
Fetter, N.L., Leddy, H.A., Guilak, F., Nunley, J.A., 2006. Composition and transport properties of human ankle and knee cartilage. Journal of Orthopaedic Research 24 (2), 211–219.
Greene, G.W., Zappone, B., Zhao, B., Soderman, O., Topgaard, D., Rata, G., Israelachvili, J.N., 2008. Changes in pore morphology and fluid transport in compressed articular cartilage and the implications for joint lubrication. Biomaterials 29 (33), 4455–4462.

Guilak, F., Jones, W.R., Ting-Beall, H.P., Lee, G.M., 1999. The deformation behavior and mechanical properties of chondrocytes in articular cartilage. Osteoarthritis Cartilage 7 (1), 59–70.
Guterl, C.C., Gardner, T.R., Rajan, V., Ahmad, C.S., Hung, C.T., Ateshian, G.A., 2009. Two-dimensional strain fields on the cross-section of the human patellofemoral joint under physiological loading. Journal of Biomechanics 42 (9), 1275–1281.
Irrechukwu, O.N., 2007. The Role of Matrix Composition and Age in Solute Diffusion within Articular Cartilage. Ph.D. Thesis. Georgia Institute of Technology, Atlanta.
Jadin, K.D., Wong, B.L., Bae, W.C., Li, K.W., Williamson, A.K., Schumacher, B.L., Price, J.H., Sah, R.L., 2005. Depth-varying density and organization of chondrocytes in immature and mature bovine articular cartilage assessed by 3d imaging and analysis. Journal of Histochemistry and Cytochemistry 53 (9), 1109–1119.
Kaapa, A., Peter, K., Ylanne, J., 1999. Effects of mutations in the cytoplasmic domain of integrin beta(1) to talin binding and cell spreading. Experimental Cell Research 250 (2), 524–534.
Leddy, H.A., Christensen, S.E., Guilak, F., 2008. Microscale diffusion properties of the cartilage pericellular matrix measured using 3D scanning microphotolysis. Journal of Biomechanical Engineering 130 (6), 061002.
Lefebvre, V., Garofalo, S., Zhou, G., Metsaranta, M., Vuorio, E., Crombrugghe, B.De, 1994. Characterization of primary cultures of chondrocytes from type II collagen/beta-galactosidase transgenic mice. Matrix Biology 14 (4), 329–335.
Loeser, R.F., 1997. Growth factor regulation of chondrocyte integrins. Differential effects of insulin-like growth factor 1 and transforming growth factor beta on alpha 1 beta 1 integrin expression and chondrocyte adhesion to type VI collagen. Arthritis and Rheumatism 40 (2), 270–276.
Loeser, R.F., 2000. Chondrocyte integrin expression and function. Biorheology 37 (1–2), 109–116.
Maroudas, A., 1970. Distribution and diffusion of solutes in articular cartilage. Biophysical Journal 10 (5), 365–379.
Maroudas, A., 1979. Physicochemical properties of articular cartilage. In: Freeman, M.A.R. (Ed.), In Adult Articular Cartilage. Pitman Medical, Bath, pp. 215–290.
Otey, C.A., Vasquez, G.B., Burridge, K., Erickson, B.W., 1993. Mapping of the alpha-actinin binding site within the beta 1 integrin cytoplasmic domain. Journal of Biological Chemistry 268 (28), 21193–21197.
Poole, C.A., Ayad, S., Schofield, J.R., 1988. Chondrons from articular cartilage: I. Immunolocalization of type VI collagen in the pericellular capsule of isolated canine tibial chondrons. Journal of Cell Science 90 (Pt 4), 635–643.
Potocnik, A.J., Brakebusch, C., Fassler, R., 2000. Fetal and adult hematopoietic stem cells require beta1 integrin function for colonizing fetal liver, spleen, and bone marrow. Immunity 12 (6), 653–663.
Raducanu, A., Hunziker, E.B., Drosse, I., Aszodi, A., 2009. Beta1 integrin deficiency results in multiple abnormalities of the knee joint. Journal of Biological Chemistry 284 (35), 23780–23792.
Rosenberg, L., 1971. Chemical basis for the histological use of safranin O in the study of articular cartilage. Journal of Bone and Joint Surgery American 53 (1), 69–82.
Sakai, K., Hiripi, L., Glumoff, V., Brandau, O., Eerola, R., Vuorio, E., Bosze, Z., Fassler, R., Aszodi, A., 2001. Stage- and tissue-specific expression of a Col2a1–Cre fusion gene in transgenic mice. Matrix Biology 19 (8), 761–767.
Stockwell, R.A., 1972. Inter-relationship of articular cartilage thickness and cellularity. Annals of the Rheumatic Diseases 31 (5), 424.
Torzilli, P.A., Arduino, J.M., Gregory, J.D., Bansal, M., 1997. Effect of proteoglycan removal on solute mobility in articular cartilage. Journal of Biomechanics 30 (9), 895–902.
Trampel, R., Schiller, J., Naji, L., Stallmach, F., Karger, J., Arnold, K., 2002. Self-diffusion of polymers in cartilage as studied by pulsed field gradient NMR. Biophysical Chemistry 97 (2–3), 251–260.
Wickstrom, S.A., Fassler, R., 2011. Regulation of membrane traffic by integrin signaling. Trends in Cell Biology 21 (5), 266–273.